

Multi-View Spectral Clustering Tailored Tensor Low-Rank Representation

Yuheng Jia, Hui Liu, Junhui Hou, *Senior Member, IEEE*, Sam Kwong, *Fellow, IEEE*, and Qingfu Zhang, *Fellow, IEEE*

Abstract—This paper explores the problem of multi-view spectral clustering (MVSC) based on tensor low-rank modeling. Unlike the existing methods that all adopt an off-the-shelf tensor low-rank norm without considering the special characteristics of the tensor in MVSC, we design a novel structured tensor low-rank norm tailored to MVSC. Specifically, we explicitly impose a symmetric low-rank constraint and a structured sparse low-rank constraint on the frontal and horizontal slices of the tensor to characterize the intra-view and inter-view relationships, respectively. Moreover, the two constraints could be jointly optimized to achieve mutual refinement. On basis of the novel tensor low-rank norm, we formulate MVSC as a convex low-rank tensor recovery problem, which is then efficiently solved with an augmented Lagrange multiplier based method iteratively. Extensive experimental results on five benchmark datasets show that the proposed method outperforms state-of-the-art methods to a significant extent. Impressively, our method is able to produce perfect clustering. In addition, the parameters of our method can be easily tuned, and the proposed model is robust to different datasets, demonstrating its potential in practice.

Index Terms—Multi-view spectral clustering, tensor low-rank representation, tensor low-rank norm.

I. INTRODUCTION

As a promising tool to analyze data, spectral clustering (SC) [1], which exploits the pairwise relationship between samples, was initially designed for the single-view data. However, many real-world datasets may be collected via multi-modalities or diverse feature extractors [2]. For example, a self-driving car has a series of sensors to sense the road conditions. An image can be represented by different types of features, e.g., texture, color, and edge. Those multi-view features can provide enormous information about the dataset, and the features from different views depict the dataset from different perspectives that may be complementary to each other. Thus, many multi-view spectral clustering (MVSC) methods were proposed [3] for processing such multi-view data. For example, Xia *et al.* [4] first constructed a set of similarity matrices from multiple views, and then decomposed those matrices into a shared similarity matrix for the final clustering task and a series of sparse error matrices. Cao *et al.* [5] proposed to explore the complementary information by a novel diversity-induced

term. Zhao *et al.* [6] realized MVSC with a non-negative matrix factorization approach. Zhang *et al.* [7] learned a latent representation for multiple features, and simultaneously performed data reconstruction based on the learned latent representation. Wang *et al.* [8] explored the complementarity as well as the consistency among different views at the same time. See [9], [10], [11] for the comprehensive surveys on MVSC.

Recently, by stacking the similarity matrices from multiple views as a 3-dimensional (3-D) tensor, tensor based MVSC methods [12] have received considerable attention. Specifically, by exploiting the low-rankness of the tensor, this kind of methods can automatically capture the higher-order correlations beneath the multiple features. For example, Zhang *et al.* [13] proposed a low-rank tensor constrained self-representation model for MVSC, where the tensor low-rank norm was proposed by [14]. Xie *et al.* [15] extended the work of [13] with a different tensor low-rank norm defined by tensor singular value decomposition (SVD) [16]. More importantly, the tensor is rotated to ensure the consensus among multiple views, which improves clustering performance to a new level, compared with the previous methods. Wu *et al.* [17] proposed to learn a low-rank tensor for SC directly from a set of multiple similarity matrices. Qu *et al.* [18] kernelized original data to explore the non-linear relationships among samples under the tensor MVSC framework [15]. Tensor based MVSC methods were also extended to solve the time series clustering problem [19].

Although the above-mentioned tensor based MVSC methods have improved clustering performance to some extent, all of them adopt an existing tensor low-rank norm (TLRN), which is designed for general purposes without taking the unique characteristics of MVSC into account. That is, the existing TLRNs describe the relationships among entries of a tensor from a global perspective; however, the tensor constructed by multiple similarity matrices in MVSC has some unique local structures. To this end, we propose a novel TLRN tailored to MVSC, and then formulate the MVSC as a low-rank tensor learning problem. Specifically, as shown in Fig. 1, ideally, the frontal slices of the tensor that capture the intra-view relationships among samples should be block-diagonal matrices, while the horizontal and lateral slices of the tensor, which capture the inter-view relationships of a typical sample from diverse views, should be column/row-wise sparse matrices. To pursue such unique characteristics, we propose a novel TLRN tailored to MVSC, which explicitly imposes a symmetric low-rank constraint and a column-wise sparse

Y. Jia and H. Liu are with the Department of Computer Science, City University of Hong Kong, Kowloon, Hong Kong. (e-mail: yuheng.jia@my.cityu.edu.hk; hliu99-c@my.cityu.edu.hk).

J. Hou, S. Kwong and Q. Zhang are with the Department of Computer Science, City University of Hong Kong, Kowloon, Hong Kong and also with the City University of Hong Kong Shenzhen Research Institute, Shenzhen, 51800, China, (e-mail: jh.hou@cityu.edu.hk; cssamk@cityu.edu.hk; qingfu.zhang@cityu.edu.hk).

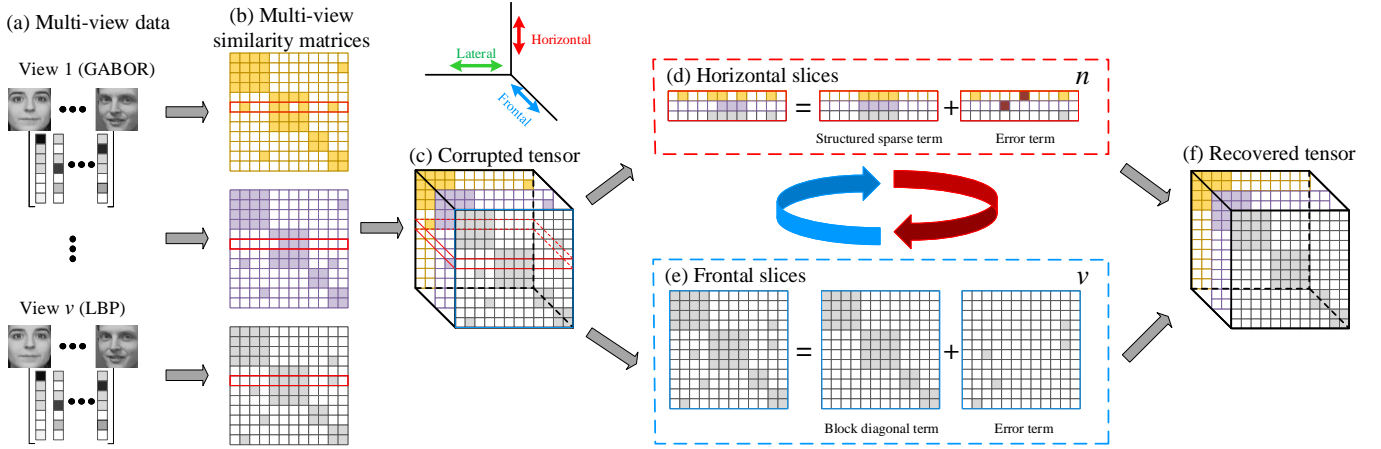


Fig. 1. Visual illustration of the proposed model. Given the input data with v views (a), v similarity matrices of each corresponding to a view are first constructed with a typical method (b). Then, the resulting similarity matrices are stacked to form a corrupted tensor (c). Taking the characteristics of multi-view clustering into consideration, the slices of the tensor along different dimensions own different special structures. Specifically, for the frontal slices that correspond the similarity relationships within a view, they exhibit a block-diagonal appearance (e). For the horizontal slices that correspond to sample-level relationships across different views, they should be structured sparse matrices, i.e., column-wise sparse (all the entries of some columns are zero) (d). We impose a symmetric low-rank term and a structured sparse low-rank term on the frontal and horizontal slices, respectively, to seek the ideal appearances. More importantly, the two types of low-rank representations are performed simultaneously to mutually boost each other. Finally, an enhanced low-rank tensor representation tailored to MVSC can be achieved (f).

low rank constraint to the frontal and horizontal slices¹ of the tensor, respectively. Moreover, these two constraints are implemented simultaneously to achieve mutual enhancement. Based on the MVSC tailored TLRN, we formulate MVSC as a convex low-rank tensor recovery problem, which can be efficiently solved with an augmented Lagrange multiplier method. We validate the proposed model on five commonly-used multi-view clustering datasets, and experimental results show that the proposed model can dramatically improve state-of-the-art methods. More impressively, our model is able to produce perfect or nearly perfect clustering. We believe our perspective on MVSC will inspire this community.

The rest of this paper is organized as follows. In Section II, we briefly review existing TLRNs and related MVSC methods. Section III presents the proposed TLRN and the associated model for MVSC as well as its numerical solution. In Section IV, we validate the advantages of the proposed method with extensive experiments. Finally, Section V concludes this paper and discusses several future works.

II. RELATED WORK

A. Tensor Low-Rank Norm (TLRN)

As a generalization of matrices, tensors are higher order multidimensional arrays. Rank is one of the most fundamental characteristics of a matrix. Unlike that of a matrix, the rank of a tensor is, however, not unique, and different tensor ranks were induced by different kinds of tensor decompositions [20], [21]. For example, the CANDECOMP/PARAFAC (CP) rank was induced by the CP decomposition [22], which factorizes a tensor as a linear combination of rank-one tensors. However, estimating the CP rank of a tensor is an NP-hard problem

¹When the frontal slices are symmetric matrices, the horizontal slices will be the same as the transpose of the lateral slices.

[23]. As an alternative, the Tucker rank is a vector [14], the i -th element of which is the rank of the mode- i matricization of the tensor. Liu *et al.* [14] proposed using the sum of nuclear norms (SNN) to relax the discrete and non-convex Tucker rank. Specifically, taking a 3-D tensor $\mathcal{A} \in \mathbb{R}^{n_1 \times n_2 \times n_3}$ as an example, SNN is defined as

$$\text{SNN}(\mathcal{A}) = \sum_{m=1}^3 \zeta_m \|\mathbf{A}_m\|_*, \quad (1)$$

where $\mathbf{A}_m \in \mathbb{R}^{n_m \times (\frac{n_1 n_2 n_3}{n_m})}$ is a matrix by unfolding \mathcal{A} along the m -th mode ($m = 1, 2,$ and 3), ζ_m is the weight corresponding to the m -th mode, and $\|\cdot\|_*$ returns the nuclear norm of a matrix.

Recently, the tensor tubal rank was induced based on tensor SVD (t-SVD) [16]. Specifically, t-SVD is represented as

$$\mathcal{A} = \mathcal{U} \star \mathcal{S} \star \mathcal{V}, \quad (2)$$

where $\mathcal{U} \in \mathbb{R}^{n_1 \times n_1 \times n_3}$ and $\mathcal{V} \in \mathbb{R}^{n_2 \times n_2 \times n_3}$ are orthogonal tensors, $\mathcal{S} \in \mathbb{R}^{n_1 \times n_2 \times n_3}$ is an F-diagonal tensor, and \star denotes the tensor-to-tensor product. The detailed definitions of those tensor operators can be found in [24]. According to t-SVD, the tubal rank is defined as the number of non-zero tubes in \mathcal{S} , i.e.,

$$\text{tubal rank}(\mathcal{A}) = \#\{i, \mathcal{S}(i, i, :) \neq 0\}. \quad (3)$$

Then, Zhang *et al.* [25] proposed a tensor nuclear norm using the t-SVD defined as

$$\|\mathcal{A}\|_{\text{tSVD}} = \sum_{i=1}^{\min(n_1, n_2)} \sum_{k=1}^{n_3} |\mathcal{S}(i, i, k)|, \quad (4)$$

and Lu *et al.* [24] also proposed a novel tensor nuclear norm based on t-SVD, but only used the first frontal slice of \mathcal{S} , i.e.,

$$\|\mathcal{A}\|_{\text{tSVD}_{\text{ff}}} = \sum_i \mathcal{S}(i, i, 1). \quad (5)$$

Such a definition makes it consistent with the matrix nuclear norm [24].

B. Mult-View Spectral Clustering (MVSC)

According to the involvement of TLRNs, we roughly divide existing MVSC methods into two categories, i.e., the non-tensor methods and tensor based methods.

For the first category, one commonly adopted strategy is to exploit the consensus among all the views [26], [6]. For example, Kumar *et al.* [27] proposed to learn a common representation from all the views. Xia *et al.* [4] recovered a shared low-rank matrix from multiple input similarity matrices as the final affinity matrix for clustering. Since different views may contain valuable individual information, exploring the complementary information among them is also important. For example, a co-training method was proposed to alternatively use the clustering result from one view to guide the other [28]. Cao *et al.* [5] used the Hilbert Schmidt Independence Criterion as a diversity term to exploit complementary of multiple views. Moreover, some works tried to simultaneously use both the consistency and complementary information among different views [29], [8] to further improve the clustering performance. Besides, MVSC was also exploited in the latent space [30], [31].

By concatenating the similarity matrices from multiple views to form a 3-D tensor, many tensor based MVSC methods were proposed [13]. This kind of methods is appealing since by exploring the low-rankness of the formed tensor, the original similarity matrices can be complemented and refined from a higher-order perspective, such that both the consistency and complementarity between different views are taken into consideration naturally. Zhang *et al.* [13] proposed the first tensor based MVSC method, which is formulated as

$$\begin{aligned} & \min_{\mathbf{Z}^i, \mathbf{E}^i} \text{SNN}(\mathcal{Z}) + \lambda \|\mathbf{E}\|_{2,1} \\ \text{s.t. } & \mathbf{X}^i = \mathbf{X}^i \mathbf{Z}^i + \mathbf{E}^i, i = 1, 2, \dots, v, \\ & \mathcal{Z} = \Phi(\mathbf{Z}^1, \mathbf{Z}^2, \dots, \mathbf{Z}^v), \\ & \mathbf{E} = [\mathbf{E}^1; \mathbf{E}^2; \dots; \mathbf{E}^v], \end{aligned} \quad (6)$$

where $\{\mathbf{X}^i\} \in \mathbb{R}^{d_i \times n}$, $i = 1, 2, \dots, v$ are the data matrices from different views with d_i , n , and v being the dimension of the features of the i th view, the number of samples, and the number of views, respectively, $\{\mathbf{Z}^i\} \in \mathbb{R}^{n \times n}$, $i = 1, 2, \dots, v$ are the learned similarity matrices from different views, $\{\mathbf{E}^i\} \in \mathbb{R}^{d_i \times n}$, $i = 1, 2, \dots, v$ denote the set of error matrices of all views, $\Phi(\cdot)$ is a function merging the similarity matrices $\{\mathbf{Z}^i\}$ to form a 3-D tensor $\mathcal{Z} \in \mathbb{R}^{n \times n \times v}$, $\mathbf{E} \in \mathbb{R}^{\sum_i d_i \times n}$ concatenates all the error matrices $\{\mathbf{E}^i\}$ together along the column, $\|\cdot\|_{2,1}$ is the column-wise $\ell_{2,1}$ norm of matrix², and $\lambda > 0$ is the hyper-parameter to balance the error term and the low-rank term. By solving Eq. (6), the SNN is minimized

to characterize the view-to-view relationship. Then, Xie *et al.* [15] extended Eq. (6) by using t-SVD, i.e.,

$$\begin{aligned} & \min_{\mathbf{Z}^i, \mathbf{E}^i} \|\mathcal{Z}\|_{\text{tSVD}} + \lambda \|\mathbf{E}\|_{2,1} \\ \text{s.t. } & \mathbf{X}^i = \mathbf{X}^i \mathbf{Z}^i + \mathbf{E}^i, i = 1, 2, \dots, v, \\ & \mathcal{Z} = \Phi(\mathbf{Z}^1, \mathbf{Z}^2, \dots, \mathbf{Z}^v) \\ & \mathbf{E} = [\mathbf{E}^1; \mathbf{E}^2; \dots; \mathbf{E}^v]. \end{aligned} \quad (7)$$

It is noteworthy that [15] rotates the tensor \mathcal{Z} to better exploit the view-to-view relationship. With the same TLRN as [15], Wu *et al.* [17] realized MVSC with a robust tensor principal component analysis approach, i.e.,

$$\begin{aligned} & \min_{\mathcal{Z}, \mathcal{E}} \|\mathcal{Z}\|_{\text{tSVD}} + \lambda \|\mathcal{E}\|_1 \\ \text{s.t. } & \mathcal{W} = \mathcal{Z} + \mathcal{E}, \end{aligned} \quad (8)$$

where $\mathcal{W} \in \mathbb{R}^{n \times n \times v}$ is the input tensor constructed by the similarity matrices from different views, $\mathcal{E} \in \mathbb{R}^{n \times n \times v}$ is the error tensor, and $\|\mathcal{E}\|_1 = \sum_{ijk} |\mathcal{E}(i, j, k)|$ denotes the ℓ_1 norm of a tensor. Yin *et al.* [12] used the TLRN in [24] to achieve MVSC, i.e.,

$$\begin{aligned} & \min_{\mathcal{Z}} \|\mathcal{Z}\|_{\text{tSVD}_{\text{ff}}} + \lambda \|\mathcal{X} - \mathcal{X} \star \mathcal{Z}\|_F^2 + \alpha \|\mathcal{Z}\|_1 \\ & \quad + \beta \sum_{i \neq j} \|\mathcal{Z}(:, :, i) - \mathcal{Z}(:, :, j)\|_F^2, \end{aligned} \quad (9)$$

where \mathcal{X} is the input sample tensor, $\|\cdot\|_F$ denotes the Frobenius norm of a tensor, and λ, α, β are the hyper-parameters. Note that in Eq. (9) the tensor-to-tensor product is introduced to better explore the higher-order information among samples, and the fourth term enhances the consistency among different views. Besides, tensor based MVSC was extended in a semi-supervised manner by utilizing some prior information [32], [33].

The above-mentioned works have validated the effectiveness of exploring the low-rankness of the tensor encoding similarity relationships in MVSC. However, all of them adopt an existing TLRN without considering the special characteristics of MVSC, which may limit their performance in clustering.

III. PROPOSED METHOD

Given a multi-view dataset with n samples and v views, for each view we could build a similarity matrix³ to describe the pairwise relationships between samples, i.e., $\mathbf{W}^i \in \mathbb{R}^{n \times n}$, where $i \in \{1, 2, \dots, v\}$ is the view index. The tensor based MVSC methods stack the similarity matrices of all views to form a 3-D tensor denoted as $\mathcal{W} \in \mathbb{R}^{n \times n \times v}$, where the i -th frontal slice of \mathcal{W} is \mathbf{W}^i .

As aforementioned, the idea underlying tensor based MVSC methods is to recover a low-rank tensor $\mathcal{L} \in \mathbb{R}^{n \times n \times v}$ such that the information across diverse views and within each view is fully exploited from \mathcal{W} . To achieve the goal, all of the previous methods adopt a typical TLRN which is designed for general purposes by exploiting a tensor globally. However, the tensor constructed by multi-view similarity matrices has some special characteristics that need to be depicted locally, making the

²For a matrix $\mathbf{M} \in \mathbb{R}^{m \times n}$, $\|\mathbf{M}\|_{2,1} = \sum_{i=1}^n \|\mathbf{M}(:, i)\|_2$.

³ Commonly used similarity matrix construction methods could be found at [1].

existing TLRNs not be the best choice for MVSC. To this end, we propose a novel TLRN tailored to the MVSC task, which is capable of better characterizing the special structures of the tensor constructed by multiple similarity matrices.

A. Proposed MVSC Tailored TLRN

As can be seen from Fig. 1-(e), each frontal slice of the tensor corresponds to the intra-view similarity relationships of all the samples. In the ideal case, it should be a block-diagonal matrix, where only the samples from the same clusters are connected. To capture such a structure, we use symmetry and low-rankness to regularize the frontal slices and define

$$\begin{aligned} \|\mathcal{L}\|_{\oplus} &:= \sum_{i=1}^v \text{rank}(\mathbf{L}_f^i), \\ \text{s.t. } \mathbf{L}_f^i &= \mathbf{L}_f^{i\top}, \end{aligned} \quad (10)$$

where $\mathbf{L}_f^i \in \mathbb{R}^{n \times n}$ is the i -th frontal slice of tensor \mathcal{L} used in MVSC, and \cdot^\top and $\text{rank}(\cdot)$ denote the transpose and rank of a matrix, respectively.

Similarly, each row of the horizontal slice (or column of the lateral slice) of the tensor depicts the pairwise relationships between a typical sample and all the other samples, i.e., the horizontal slice represents the inter-view relationships of the sample. As shown in Fig. 1-(d), in the ideal case, it is a structured column-wise sparse matrix, where only a few columns are non-zero. Thus, we propose the following regularizer to model such a behavior, defined as

$$\|\mathcal{L}\|_{\otimes} := \sum_{j=1}^n \text{rank}(\mathbf{L}_h^j) + \alpha \|\mathbf{L}_h^j\|_{2,0}, \quad (11)$$

where $\mathbf{L}_h^j \in \mathbb{R}^{c \times n}$ denotes the j -th horizontal slice of \mathcal{L} , $\|\cdot\|_{2,0}$ is a column-wise sparse norm, i.e., counting the number of columns that are non-zero, and $\alpha > 0$ balances the importance of the two terms. Since we restrict the symmetry of the frontal slices in Eq. (10) and the constraints on the horizontal slices equal to the constraints on the transpose of the lateral slices, it is not necessary to add the constraints on the lateral slices.

To pursue the ideal appearance of the tensor in MVSC, we leverage the characteristics of both the intra-view and inter-view of the tensor, leading to an MVSC tailored norm:

$$\mathcal{L}_{\oplus} := \omega_1 \|\mathcal{L}\|_{\oplus} + \omega_2 \|\mathcal{L}\|_{\otimes}, \quad (12)$$

where $0 \leq \omega_1 \leq 1$ and $\omega_2 = 1 - \omega_1$ balance the contributions of $\|\mathcal{L}\|_{\oplus}$ and $\|\mathcal{L}\|_{\otimes}$. By minimizing Eq. (12), both the intra-view and inter-view relationships are optimized at the same time to boost each other.

However, in Eq.(12), the discrete and non-smooth properties of both the $\text{rank}(\cdot)$ function and the $\ell_{2,0}$ norm make it inefficient to solve. We thus relax them by their convex hulls, i.e., the unclear norm $\|\cdot\|_*$ and the $\ell_{2,1}$ norm, respectively. Finally, the proposed convex MVSC tailored TLRN is written as

$$\begin{aligned} \mathcal{L}_{\oplus} &:= \omega_1 \sum_{i=1}^v \|\mathbf{L}_f^i\|_* + \omega_2 \left(\sum_{j=1}^n \|\mathbf{L}_h^j\|_* + \alpha \|\mathbf{L}_h^j\|_{2,1} \right), \\ \text{s.t.}, \mathbf{L}_f^i &= \mathbf{L}_f^{i\top}, \forall i \in \{1, 2, \dots, v\}. \end{aligned} \quad (13)$$

Since \mathcal{L}_{\oplus} is the linear combination of two kinds of valid norms (nuclear norm and $\ell_{2,1}$ norm), the proposed MVSC tailored TLRN is also a valid norm.

B. Proposed MVSC Model

Based on the proposed TLRN in Eq. (13), we cast the MVSC as a low-rank tensor recovery problem, which is expressed as

$$\begin{aligned} \min_{\mathcal{L}, \mathcal{E}} \|\mathcal{L}\|_{\oplus} + \lambda \|\mathcal{E}\|_F^2 \\ \text{s.t.}, \mathcal{W} = \mathcal{L} + \mathcal{E}, \end{aligned} \quad (14)$$

where \mathcal{W} is an observed tensor with corruptions, $\mathcal{E} \in \mathbb{R}^{n \times n \times v}$ is the noise error tensor, $\|\cdot\|_F$ extends the matrix Frobenius norm to a tensor case, i.e., $\|\mathcal{E}\|_F = \sqrt{\sum_{ijk} \mathcal{E}_{ijk}^2}$, and λ is a positive penalty parameter. By optimizing Eq. (14), the recovered tensor \mathcal{L} will be encouraged to conform to the ideal appearance of a tensor constructed by the ideal similarity matrices. Then, the high clustering performance on \mathcal{L} can be expected.

Note that unlike the well-known robust principal component analysis (RPCA) [34] and tensor RPCA [24], which impose an ℓ_1 norm on the error matrix/tensor, our model adopts a Frobenius-type norm to regularize the error tensor. The reason is that a sparse regularizer on \mathcal{E} will conflict with the $\ell_{2,1}$ norm on the horizontal slices. The subsequent experimental results also validate the superiority of the proposed model.

Differences between Ours and SNN [14]. Although both our TLRN and SNN are the sum of matrix nuclear norms, they are essentially different. Specifically, the involved matrices in SNN are the matricization of a tensor along different modes. While, the matrices in our TLRN are the frontal and horizontal slices of a tensor. In addition, we impose a symmetric constraint and a column-wise sparse constraint on the frontal and horizontal slices, respectively. Such a different mathematic expression reveals the essential difference between them, i.e., the proposed TLRN is tailored to MVSC by seeking the ideal appearance for the tensor constructed by multiple similarity matrices, while SNN is just a relaxation of the tensor Tucker rank for general low-rankness. As will be shown in Section IV-B, the significant superiority of our method in terms of clustering performance over SNN and other TLRNs substantiates that the proposed TLRN is indeed tailored to MVSC.

C. Optimization Algorithm

We use the inexact augmented Lagrange multiplier (IALM) [35] method to solve the resulting convex model in Eq. (14). Specifically, the IALM converts the original problem into several smaller sub-problems, each of which is relatively easier to solve. By introducing three auxiliary tensors, i.e., $\mathcal{L}_1 = \mathcal{L}_2 = \mathcal{L}_3 = \mathcal{L}$, Eq. (14) is equivalently rewritten as

$$\begin{aligned} \min_{\mathcal{L}_1, \mathcal{L}_2, \mathcal{L}_3, \mathcal{E}} \omega_1 \sum_{i=1}^v \|\mathbf{L}_{1f}^i\|_* + \omega_2 \sum_{j=1}^n \left(\|\mathbf{L}_{2h}^j\|_* + \alpha \|\mathbf{L}_{3h}^j\|_{2,1} \right) + \lambda \|\mathcal{E}\|_F^2 \\ \text{s.t. } \mathcal{W} = \mathcal{L}_k + \mathcal{E}, \mathcal{L}_k = \mathcal{L}, \forall k \in \{1, 2, 3\}, \mathbf{L}_1^i = \mathbf{L}_1^{i\top}, \forall i \in \{1, \dots, v\}. \end{aligned} \quad (15)$$

The augmented Lagrange form of Eq. (15) is

$$\begin{aligned} \underset{\substack{\mathcal{L}_1, \mathcal{L}_2, \\ \mathcal{L}_3, \mathcal{L}, \mathcal{E}}}{\text{argmin}} & \omega_1 \sum_{i=1}^v \|\mathbf{L}_{1f}^i\|_* + \omega_2 \sum_{j=1}^n \left(\|\mathbf{L}_{2h}^j\|_* + \alpha \|\mathbf{L}_{3h}^j\|_{2,1} \right) + \lambda \|\mathcal{E}\|_F^2 \\ & + \sum_{k=1}^3 \left(\frac{\mu}{2} \left\| \mathcal{W} - \mathcal{L}_k - \mathcal{E} + \frac{\mathcal{Y}_{1k}}{\mu} \right\|_F^2 + \frac{\mu}{2} \left\| \mathcal{L} - \mathcal{L}_k + \frac{\mathcal{Y}_{2k}}{\mu} \right\|_F^2 \right) \\ \text{s.t.}, & \mathbf{L}_1^i = \mathbf{L}_1^{iT}, \forall i \in \{1, \dots, v\}, \end{aligned} \quad (16)$$

where $\mu > 0$ introduces the Lagrange multiplier terms, and $\mathcal{Y}_{1k} \in \mathbb{R}^{n \times n \times v}$, $k \in \{1, 2, 3\}$ and $\mathcal{Y}_{2k} \in \mathbb{R}^{n \times n \times v}$, $k \in \{1, 2, 3\}$ are the Lagrange multipliers. The IALM splits Eq. (16) into several sub-problems, and iteratively solves those sub-problems until convergence.

Specifically, the \mathcal{E} sub-problem is written as

$$\min_{\mathcal{E}} \lambda \|\mathcal{E}\|_F^2 + \sum_{k=1}^3 \frac{\mu}{2} \left\| \mathcal{W} - \mathcal{L}_k - \mathcal{E} + \frac{\mathcal{Y}_{1k}}{\mu} \right\|_F^2, \quad (17)$$

which is a set of unconstrained quadratic equations in element-wise. Therefore, the closed-form solution is obtained as

$$\mathcal{E} = \mu \sum_{k=1}^3 \left(\mathcal{W} - \mathcal{L}_k + \frac{\mathcal{Y}_{1k}}{\mu} \right) / (2\lambda + 3\mu). \quad (18)$$

The \mathcal{L} sub-problem is written as

$$\min_{\mathcal{L}} \sum_{k=1}^3 \frac{\mu}{2} \left\| \mathcal{L} - \mathcal{L}_k + \frac{\mathcal{Y}_{2k}}{\mu} \right\|_F^2, \quad (19)$$

which is also a set of unconstrained quadratic equations with the closed-form solution:

$$\mathcal{L} = \frac{1}{3} \sum_{k=1}^3 \left(\mathcal{L}_k - \frac{\mathcal{Y}_{2k}}{\mu} \right). \quad (20)$$

For \mathcal{L}_k , $k \in \{1, 2, 3\}$ sub-problems, removing the irrelevant terms, we have

$$\begin{aligned} \min_{\mathcal{L}_k} & \frac{1}{2\mu} f(\mathcal{L}_k) + \frac{1}{2} \left\| \mathcal{L}_k - \frac{1}{2} \left(\mathcal{W} + \mathcal{L} - \mathcal{E} + \frac{\mathcal{Y}_{1k} + \mathcal{Y}_{2k}}{\mu} \right) \right\|_F^2 \\ \text{s.t.}, & \mathbf{L}_1^i = \mathbf{L}_1^{iT}, \forall i \in \{1, \dots, v\}, \end{aligned} \quad (21)$$

where $f(\mathcal{L}_1) = \omega_1 \sum_{i=1}^v \|\mathbf{L}_{1f}^i\|_*$, $f(\mathcal{L}_2) = \omega_2 \sum_{j=1}^n \|\mathbf{L}_{2h}^j\|_*$, and $f(\mathcal{L}_3) = \omega_2 \alpha \sum_{j=1}^n \|\mathbf{L}_{3h}^j\|_{2,1}$. These three sub-problems are symmetric unclear norm minimization, unclear norm minimization, and $\ell_{2,1}$ norm minimization problems, each of which has a closed-form solution, i.e.,

$$\mathcal{L}_1(:, :, i) = \mathbf{U}_f^i \mathcal{T} \left(\sum_f^i - \frac{\omega_1}{2\mu} \mathbf{I}_n \right) \mathbf{V}_f^i, \quad i = 1, 2, \dots, v, \quad (22)$$

$$\mathcal{L}_2(:, j, :) = \mathbf{U}_h^j \mathcal{T} \left(\sum_h^j - \frac{\omega_2}{2\mu} \mathbf{I}_v \right) \mathbf{V}_h^j, \quad j = 1, 2, \dots, n, \quad (23)$$

and

$$\mathcal{L}_3(:, j, p) = \begin{cases} \frac{\|\mathcal{A}_3(:, j, p)\|_2 - \frac{\omega_2 \alpha}{2\mu}}{\|\mathcal{A}_3(:, j, p)\|_2} \mathcal{A}_3(:, j, p), & \text{if } \frac{\omega_2 \alpha}{2\mu} < \|\mathcal{A}_3(:, j, p)\|_2 \\ 0, & \text{otherwise,} \end{cases} \quad j = 1, 2, \dots, n, \forall p, \quad (24)$$

Algorithm 1 Optimization Solution to Eq. (14)

Input: Similarity matrix sets $\{\mathbf{W}^i|_{i=1}^v\}$, ω_1 , λ , α ;

Initialize: $\omega_2 = 1 - \omega_1$, $\mathcal{L} = \mathcal{L}_k = \mathcal{Y}_{1k} = \mathcal{Y}_{2k} = \mathcal{O}^{n \times n \times v}$, $\forall k$, $\mu = 10^{-4}$, $\mu_{\max} = 10^8$, where \mathcal{O} denotes a tensor with all entries equal to zeros;

1: Form a tensor \mathcal{W} by stacking $\{\mathbf{W}^i|_{i=1}^v\}$;

2: **while** not converged **do**

3: Update \mathcal{L}_k , $k \in \{1, 2, 3\}$ by Eqs. (22)-(24);

4: Update \mathcal{L} by Eq. (20);

5: Update \mathcal{E} by Eq. (18);

6: Update \mathcal{Y}_{1k} , \mathcal{Y}_{2k} , $k \in \{1, 2, 3\}$ and μ by Eq. (25);

7: **end while**

8: **Output:** \mathcal{L} .

TABLE I
DATASET SUMMARY

Dataset	Samples	Views	Clusters	Type
Coil20	1440	3	20	Object
Yale	165	3	15	Face
YaleB	640	3	10	Face
ORL	400	3	40	Face
UCI-digit	2000	3	10	Digit

where $\mathbf{U}_f^i \sum_f^i \mathbf{V}_f^i$, $i = 1, \dots, v$ and $\mathbf{U}_h^j \sum_h^j \mathbf{V}_h^j$, $j = 1, \dots, n$ denote the SVD of $\frac{1}{2} (\mathcal{A}_1(:, :, i) + \mathcal{A}_1(:, :, i)^T)$, $i = 1, 2, \dots, v$ and $\mathcal{A}_2(:, j, :)$, $j = 1, 2, \dots, n$, respectively, $\mathcal{A}_k = \mathcal{W} + \mathcal{L} - \mathcal{E} + \frac{\mathcal{Y}_{1k} + \mathcal{Y}_{2k}}{\mu}$, $k \in \{1, 2, 3\}$, \mathbf{I}_n and \mathbf{I}_v are the identity matrices of size $n \times n$ and $v \times v$, respectively, $\|\cdot\|_2$ denotes the ℓ_2 norm of a vector, and $\mathcal{T}(\cdot)$ is a thresholding operator in element-wise, i.e., $\mathcal{T}(x) := \max(0, x)$.

The Lagrange multipliers and μ are updated via

$$\begin{cases} \mathcal{Y}_{1k} = \mathcal{W} - \mathcal{L}_k - \mathcal{E}, \forall k \in \{1, 2, 3\} \\ \mathcal{Y}_{2k} = \mathcal{L} - \mathcal{L}_k, \forall k \in \{1, 2, 3\} \\ \mu = \min(1.1 * \mu, \mu_{\max}), \end{cases} \quad (25)$$

where μ_{\max} gives an upper bound for μ . Finally, the overall optimization procedure is summarized in Algorithm 1.

After solving Eq. (14), we could construct the final similarity matrix by averaging \mathcal{L} along the frontal direction, i.e., $\mathbf{S} = \frac{1}{v} \sum_i \mathbf{L}_f^i$ and perform SC on \mathbf{S} to generate the clustering result.

D. Computational Complexity Analysis

The computational complexity of Algorithm 1 is dominated by step 3 which involves two nuclear norm minimization problems regarding \mathcal{L}_1 and \mathcal{L}_2 and one $\ell_{2,1}$ norm minimization problem regarding \mathcal{L}_3 . The \mathcal{L}_1 sub-problem needs to solve v SVDs of $n \times n$ matrices, which leads to a computational complexity of $O(vcn^2)$ with partial SVD [36], where c is the number of clusters. The \mathcal{L}_2 sub-problem involves n SVDs of $v \times n$ matrices resulting in a total complexity of $O(v^2n^2)$. The complexity of \mathcal{L}_3 sub-problem is much lower than those of the \mathcal{L}_1 and \mathcal{L}_2 sub-problems. Therefore, the total computational complexity of Algorithm 1 is $O(v^2n^2 + cvn^2)$.

TABLE II

CLUSTERING RESULTS (MEAN \pm STD) ON **Coil20**. WE SET $\omega_1 = 0.5$, $\alpha = 5$, AND $\lambda = 15$ IN THE PROPOSED METHOD. THE HIGHEST AND THE SECOND HIGHEST VALUES UNDER EACH METRIC ARE **BOLDED** AND UNDERLINED, RESPECTIVELY.

Method	ACC	NMI	ARI	F1-score	Precision	Recall	Purity
L-MSC [30]	0.736 \pm 0.017	0.807 \pm 0.013	0.661 \pm 0.022	0.67 \pm 0.021	0.64 \pm 0.024	0.715 \pm 0.017	0.767 \pm 0.012
DiMSC [5]	0.694 \pm 0.015	0.728 \pm 0.010	0.587 \pm 0.015	0.608 \pm 0.014	0.589 \pm 0.016	0.629 \pm 0.013	0.701 \pm 0.015
MCLES [31]	0.706 \pm 0.026	0.740 \pm 0.019	0.521 \pm 0.032	0.553 \pm 0.029	0.505 \pm 0.036	0.611 \pm 0.021	0.709 \pm 0.026
AWP [26]	0.896 \pm 0.000	0.968 \pm 0.000	0.892 \pm 0.000	0.897 \pm 0.000	0.847 \pm 0.000	0.954 \pm 0.000	0.915 \pm 0.000
<u>LT-MSC [13]</u>	<u>0.770 \pm 0.013</u>	<u>0.873 \pm 0.005</u>	<u>0.725 \pm 0.018</u>	<u>0.740 \pm 0.017</u>	<u>0.696 \pm 0.027</u>	<u>0.790 \pm 0.005</u>	<u>0.817 \pm 0.005</u>
Ut-SVD-MSC [15]	0.794 \pm 0.015	0.877 \pm 0.005	0.755 \pm 0.018	0.767 \pm 0.017	0.746 \pm 0.025	0.790 \pm 0.009	0.818 \pm 0.009
t-SVD-MSC [15]	0.836 \pm 0.007	0.924 \pm 0.002	0.799 \pm 0.011	0.810 \pm 0.010	0.759 \pm 0.021	0.869 \pm 0.003	0.879 \pm 0.001
ETLMC [17]	0.956 \pm 0.037	0.977 \pm 0.012	0.950 \pm 0.035	0.952 \pm 0.033	0.937 \pm 0.049	0.969 \pm 0.019	0.965 \pm 0.027
SCMV-3DT [12]	0.761 \pm 0.011	0.857 \pm 0.004	0.707 \pm 0.013	0.722 \pm 0.013	0.685 \pm 0.017	0.764 \pm 0.010	0.802 \pm 0.007
SNN [14]	0.850 \pm 0.016	0.927 \pm 0.005	0.819 \pm 0.021	0.828 \pm 0.020	0.788 \pm 0.034	0.874 \pm 0.008	0.885 \pm 0.007
TRPCA [24]	0.853 \pm 0.018	0.906 \pm 0.004	0.818 \pm 0.016	0.827 \pm 0.015	0.805 \pm 0.021	0.851 \pm 0.008	0.882 \pm 0.010
Proposed	1.000 \pm 0.000						

TABLE III

CLUSTERING RESULTS (MEAN \pm STD) ON **YALE**. WE SET $\omega_1 = 0.5$, $\alpha = 5$, AND $\lambda = 15$ IN THE PROPOSED METHOD.

Method	ACC	NMI	ARI	F1-score	Precision	Recall	Purity
L-MSC [30]	0.735 \pm 0.022	0.741 \pm 0.012	0.528 \pm 0.019	0.559 \pm 0.018	0.518 \pm 0.019	0.607 \pm 0.019	0.735 \pm 0.022
DiMSC [5]	0.694 \pm 0.016	0.694 \pm 0.013	0.505 \pm 0.021	0.536 \pm 0.020	0.523 \pm 0.022	0.549 \pm 0.018	0.698 \pm 0.014
MCLES [31]	0.706 \pm 0.026	0.740 \pm 0.019	0.521 \pm 0.032	0.553 \pm 0.029	0.505 \pm 0.036	0.611 \pm 0.021	0.708 \pm 0.026
AWP [26]	0.587 \pm 0.000	0.601 \pm 0.000	0.309 \pm 0.000	0.364 \pm 0.000	0.278 \pm 0.000	0.529 \pm 0.000	0.587 \pm 0.000
<u>LT-MSC [13]</u>	<u>0.739 \pm 0.014</u>	<u>0.767 \pm 0.009</u>	<u>0.597 \pm 0.013</u>	<u>0.623 \pm 0.012</u>	<u>0.601 \pm 0.012</u>	<u>0.647 \pm 0.014</u>	<u>0.739 \pm 0.014</u>
Ut-SVD-MSC [15]	0.732 \pm 0.007	0.762 \pm 0.008	0.580 \pm 0.016	0.607 \pm 0.015	0.576 \pm 0.019	0.641 \pm 0.011	0.732 \pm 0.007
t-SVD-MSC [15]	0.955 \pm 0.040	0.954 \pm 0.030	0.913 \pm 0.057	0.918 \pm 0.053	0.909 \pm 0.059	0.928 \pm 0.047	0.955 \pm 0.040
ETLMC [17]	0.677 \pm 0.074	0.725 \pm 0.062	0.558 \pm 0.089	0.585 \pm 0.083	0.572 \pm 0.085	0.599 \pm 0.082	0.677 \pm 0.074
SCMV-3DT [12]	0.711 \pm 0.007	0.731 \pm 0.008	0.530 \pm 0.013	0.560 \pm 0.012	0.536 \pm 0.014	0.587 \pm 0.011	0.716 \pm 0.006
SNN [14]	0.853 \pm 0.043	0.883 \pm 0.032	0.743 \pm 0.074	0.760 \pm 0.069	0.726 \pm 0.081	0.798 \pm 0.056	0.853 \pm 0.043
TRPCA [24]	0.760 \pm 0.039	0.787 \pm 0.034	0.629 \pm 0.049	0.652 \pm 0.046	0.633 \pm 0.044	0.673 \pm 0.050	0.767 \pm 0.037
Proposed	0.988 \pm 0.001	0.988 \pm 0.001	0.975 \pm 0.003	0.976 \pm 0.003	0.974 \pm 0.003	0.979 \pm 0.002	0.988 \pm 0.001

IV. EXPERIMENTS

A. Experiment Settings

Five commonly-used multi-view clustering image datasets were employed to evaluate the proposed model, including:

- **Coil20** is an image dataset with 20 objects, where each object has 72 samples.
- **Yale** consists of 165 face images from 15 individuals.
- **YaleB** is a face image dataset with 38 individuals, where each individual has approximate 64 images. As done in [15], we used the first 10 classes. Due to the large variation of luminance, clustering on YaleB is quite challenging.
- **ORL** is a face image datasets with 40 individuals, where each individual consists of 10 images.
- **UCI-digit** contains 2000 handwritten digits corresponding to 10 classes.

Fig. 2 shows some examples of the adopted datasets. To construct the multi-view data, for all the face and object datasets, three types of features were extracted, i.e., Gabor [37], LBP [38], and intensity. Specifically, the LBP features were extracted with the sampling density of size 8 and the uniform LBP histogram is in an (8,1) neighbourhood, and the Gabor features were extracted with one scale, 4 orientations, 39 rows and 39 columns in a 2-D gabor filter. For UCI-digit, we adopted the same features as [17], i.e., the Fourier coefficients, the morphological features and the pixel averages, to construct 3 views. Table 1 summarizes the main information of the employed datasets.

We compared the proposed method with four state-of-the-art non-tensor based MVSC methods, i.e.,

1. **L-MSC** [2020, TPAMI] [30] learns a shared latent representation from all the views and exploits the complementary information from different views simultaneously;
2. **DiMSC** [2015, CVPR] [5] learns highly diverse representations for each view to emphasize the complementary information;
3. **MCLES** [2020, AAAI] [31] is a multi-view clustering method in latent space. Besides, it could directly produce the clustering result without spectral clustering; and
4. **AWP** [2018, SIGKDD] [26] can automatically determine the importance of each view and achieve MVSC by spectral rotation.

We also compared with five state-of-the-art tensor based MVSC methods:

5. **LT-MSC** [2015, ICCV] [13] is low-rank tensor constrained self-representative model for MVSC, which uses the TLRN from [14];
6. **Ut-SVD-MSC** [2018, IJCV] [15] is an extension of LT-MSC with a different TLRN based on t-SVD [16];
7. **t-SVD-MSC** [2018, IJCV] [15] promotes the performance of Ut-SVD-MSC by rotating the original tensor to ensure the consensus among multiple views;
8. **ETLMSC** [2019, TIP] [17] is an essential tensor learning method to explore the high-order correlations for multi-view representations; and
9. **SCMV-3DT** [2019, TNNLS] [12] uses the tensor-to-

TABLE IV
CLUSTERING RESULTS (MEAN \pm STD) ON **YALEB**. WE SET $\omega_1 = 0.4$, $\alpha = 9$, AND $\lambda = 15$ IN THE PROPOSED METHOD.

Method	ACC	NMI	ARI	F1-score	Precision	Recall	Purity
L-MSC [30]	0.472 \pm 0.002	0.438 \pm 0.004	0.187 \pm 0.002	0.283 \pm 0.002	0.237 \pm 0.002	0.353 \pm 0.003	0.475 \pm 0.002
DiMSC [5]	0.520 \pm 0.003	0.496 \pm 0.003	0.32 \pm 0.004	0.393 \pm 0.004	0.375 \pm 0.004	0.412 \pm 0.003	0.523 \pm 0.003
MCLES [31]	0.426 \pm 0.001	0.420 \pm 0.001	0.129 \pm 0.001	0.240 \pm 0.001	0.185 \pm 0.001	0.344 \pm 0.001	0.426 \pm 0.001
AWP [26]	0.514 \pm 0.000	0.567 \pm 0.000	0.197 \pm 0.000	0.313 \pm 0.000	0.213 \pm 0.000	0.588 \pm 0.000	0.531 \pm 0.000
LT-MSC [13]	0.617 \pm 0.002	0.623 \pm 0.006	0.413 \pm 0.006	0.491 \pm 0.005	0.466 \pm 0.005	0.521 \pm 0.005	0.620 \pm 0.002
Ut-SVD-MSC [15]	0.502 \pm 0.001	0.506 \pm 0.001	0.236 \pm 0.001	0.325 \pm 0.001	0.276 \pm 0.001	0.395 \pm 0.001	0.503 \pm 0.001
t-SVD-MSC [15]	0.668 \pm 0.008	0.696 \pm 0.006	0.513 \pm 0.008	0.563 \pm 0.007	0.539 \pm 0.007	0.590 \pm 0.008	0.669 \pm 0.007
ETLMC [17]	0.325 \pm 0.011	0.307 \pm 0.021	0.179 \pm 0.019	0.262 \pm 0.017	0.257 \pm 0.017	0.267 \pm 0.017	0.332 \pm 0.010
SCMV-3DT [12]	0.410 \pm 0.001	0.413 \pm 0.002	0.185 \pm 0.002	0.276 \pm 0.001	0.244 \pm 0.002	0.318 \pm 0.001	0.413 \pm 0.001
SNN [14]	0.687 \pm 0.001	0.708 \pm 0.001	0.545 \pm 0.002	0.592 \pm 0.001	0.573 \pm 0.002	0.612 \pm 0.001	0.687 \pm 0.001
TRPCA [24]	0.682 \pm 0.003	0.699 \pm 0.004	0.534 \pm 0.005	0.581 \pm 0.005	0.560 \pm 0.005	0.605 \pm 0.004	0.682 \pm 0.003
Proposed	0.954 \pm 0.002	0.908 \pm 0.001	0.900 \pm 0.003	0.910 \pm 0.002	0.909 \pm 0.003	0.912 \pm 0.003	0.954 \pm 0.003

TABLE V
CLUSTERING RESULTS (MEAN \pm STD) ON **ORL**. WE SET $\omega_1 = 0.5$, $\alpha = 5$, AND $\lambda = 15$ IN THE PROPOSED METHOD.

Method	ACC	NMI	ARI	F1-score	Precision	Recall	Purity
L-MSC [30]	0.823 \pm 0.026	0.930 \pm 0.010	0.775 \pm 0.033	0.780 \pm 0.032	0.728 \pm 0.039	0.840 \pm 0.024	0.859 \pm 0.019
DiMSC [5]	0.817 \pm 0.030	0.917 \pm 0.013	0.757 \pm 0.036	0.767 \pm 0.035	0.727 \pm 0.041	0.806 \pm 0.030	0.843 \pm 0.025
MCLES [31]	0.792 \pm 0.021	0.908 \pm 0.008	0.705 \pm 0.035	0.713 \pm 0.034	0.647 \pm 0.046	0.795 \pm 0.018	0.833 \pm 0.015
AWP [26]	0.632 \pm 0.000	0.872 \pm 0.000	0.547 \pm 0.000	0.560 \pm 0.000	0.429 \pm 0.000	0.807 \pm 0.000	0.675 \pm 0.000
LT-MSC [13]	0.808 \pm 0.022	0.915 \pm 0.010	0.747 \pm 0.029	0.753 \pm 0.028	0.708 \pm 0.034	0.805 \pm 0.023	0.838 \pm 0.015
Ut-SVD-MSC [15]	0.831 \pm 0.017	0.934 \pm 0.004	0.787 \pm 0.015	0.792 \pm 0.015	0.742 \pm 0.023	0.850 \pm 0.011	0.864 \pm 0.012
t-SVD-MSC [15]	0.964 \pm 0.018	0.992 \pm 0.003	0.965 \pm 0.019	0.965 \pm 0.018	0.945 \pm 0.030	0.987 \pm 0.006	0.974 \pm 0.015
ETLMC [17]	0.946 \pm 0.018	0.986 \pm 0.005	0.942 \pm 0.020	0.943 \pm 0.019	0.918 \pm 0.026	0.970 \pm 0.014	0.960 \pm 0.014
SCMV-3DT [12]	0.839 \pm 0.012	0.908 \pm 0.007	0.763 \pm 0.018	0.769 \pm 0.017	0.747 \pm 0.020	0.792 \pm 0.016	0.852 \pm 0.012
SNN [14]	0.861 \pm 0.021	0.935 \pm 0.009	0.815 \pm 0.024	0.819 \pm 0.023	0.790 \pm 0.027	0.850 \pm 0.022	0.882 \pm 0.017
TRPCA [24]	0.932 \pm 0.015	0.978 \pm 0.005	0.922 \pm 0.017	0.924 \pm 0.016	0.896 \pm 0.022	0.954 \pm 0.013	0.947 \pm 0.011
Proposed	1.000 \pm 0.000						

TABLE VI
CLUSTERING RESULTS ON **UCI-DIGIT**. WE SET $\omega_1 = 0.4$, $\alpha = 4$, AND $\lambda = 40$ IN THE PROPOSED METHOD.

Method	ACC	NMI	ARI	F1-score	Precision	Recall	Purity
L-MSC [30]	0.899 \pm 0.000	0.819 \pm 0.000	0.795 \pm 0.000	0.816 \pm 0.000	0.812 \pm 0.000	0.819 \pm 0.000	0.899 \pm 0.000
DiMSC [5]	0.867 \pm 0.001	0.782 \pm 0.002	0.747 \pm 0.002	0.772 \pm 0.002	0.769 \pm 0.002	0.775 \pm 0.002	0.867 \pm 0.001
MCLES [31]	0.941 \pm 0.004	0.891 \pm 0.008	0.877 \pm 0.009	0.889 \pm 0.008	0.885 \pm 0.008	0.894 \pm 0.007	0.941 \pm 0.004
AWP [26]	0.871 \pm 0.000	0.899 \pm 0.000	0.835 \pm 0.000	0.853 \pm 0.000	0.783 \pm 0.000	0.937 \pm 0.000	0.872 \pm 0.000
LT-MSC [13]	0.792 \pm 0.009	0.762 \pm 0.009	0.707 \pm 0.014	0.737 \pm 0.013	0.724 \pm 0.012	0.749 \pm 0.013	0.809 \pm 0.009
Ut-SVD-MSC [15]	0.804 \pm 0.001	0.781 \pm 0.001	0.727 \pm 0.001	0.755 \pm 0.001	0.741 \pm 0.001	0.770 \pm 0.001	0.821 \pm 0.001
t-SVD-MSC [15]	0.966 \pm 0.001	0.934 \pm 0.001	0.928 \pm 0.001	0.935 \pm 0.001	0.933 \pm 0.001	0.936 \pm 0.001	0.966 \pm 0.001
ETLMC [17]	0.941 \pm 0.023	0.970 \pm 0.013	0.933 \pm 0.029	0.936 \pm 0.027	0.935 \pm 0.031	0.938 \pm 0.024	0.942 \pm 0.019
SCMV-3DT [12]	0.919 \pm 0.001	0.850 \pm 0.001	0.833 \pm 0.001	0.849 \pm 0.001	0.847 \pm 0.001	0.852 \pm 0.001	0.919 \pm 0.001
SNN [14]	0.966 \pm 0.001	0.934 \pm 0.001	0.928 \pm 0.001	0.935 \pm 0.001	0.933 \pm 0.001	0.936 \pm 0.001	0.966 \pm 0.001
TRPCA [24]	0.977 \pm 0.000	0.948 \pm 0.000	0.949 \pm 0.000	0.954 \pm 0.000	0.954 \pm 0.000	0.955 \pm 0.000	0.977 \pm 0.000
Proposed	0.998 \pm 0.000	0.993 \pm 0.000	0.994 \pm 0.000	0.995 \pm 0.000	0.995 \pm 0.000	0.995 \pm 0.000	0.998 \pm 0.000

tensor product to learn the similarity matrix for MVSC. Moreover, to illustrate the advantage of the proposed TLRN over the existing TLRNs, we also compared with two popular TLRNs:

10. **SNN** [2013, TPAMI] [14] denotes the sum of nuclear norms, which is a relaxation of tensor Tucker rank; and
11. **TRPCA** [2020, TPAMI] [24] represents the recently proposed TLRNs induced by t-SVD.

The codes of all the methods under comparison are provided by the authors. For all the methods, we used the SC method in [39] to perform clustering. For the compared MVSC methods, we exhaustively turned the hyper-parameters according to the suggested ranges by the original papers, and reported the best average results and the standard deviations (std) on 20 trials. For the proposed method and two compared TLRNs, the

initial similarity matrices of different views were initialized as those from [15]. Note that other similarity matrix construction methods can also be adopted to initialize the proposed model.

Seven metrics were adopted to evaluate the clustering results, i.e., clustering accuracy (ACC), normalized mutual information (NMI), adjusted rank index (ARI), F1-score, Precision, Recall and Purity. ARI lies in the range of $[-1, 1]$, and all the remaining metrics lie in the range of $[0, 1]$. For all metrics, larger values indicate better clustering performance, and when perfect clustering is achieved, the metrics will reach 1.

B. Comparison of Clustering Performance

Tables II-VI list clustering results of all the methods, where the most impressive observation is that our method produces the perfect clustering results on Coil20 and ORL, and almost

TABLE VII

ABLATION STUDY TOWARDS THE EFFECTIVENESS OF THE REGULARIZATION TERMS CONTAINED IN OUR METHOD. WHEN THE PARAMETER IS EQUAL TO ZERO, THE CORRESPONDING TERM IS REMOVED FROM OUR MODEL.

Coil20	ACC	NMI	ARI	F1-score	Precision	Recall	Purity
$\alpha = 0$	0.848 ± 0.018	0.928 ± 0.005	0.815 ± 0.019	0.825 ± 0.018	0.780 ± 0.031	0.875 ± 0.008	0.885 ± 0.009
$\omega_1 = 0$	0.647 ± 0.010	0.825 ± 0.005	0.409 ± 0.006	0.451 ± 0.005	0.310 ± 0.004	0.828 ± 0.012	0.721 ± 0.007
$\omega_2 = 0$	0.842 ± 0.013	0.928 ± 0.004	0.810 ± 0.018	0.820 ± 0.017	0.771 ± 0.028	0.876 ± 0.006	0.884 ± 0.006
Proposed	1.000 ± 0.000						
Yale	ACC	NMI	ARI	F1-score	Precision	Recall	Purity
$\alpha = 0$	0.849 ± 0.036	0.883 ± 0.027	0.743 ± 0.062	0.759 ± 0.058	0.725 ± 0.067	0.796 ± 0.047	0.851 ± 0.035
$\omega_1 = 0$	0.686 ± 0.011	0.747 ± 0.006	0.520 ± 0.016	0.552 ± 0.014	0.506 ± 0.020	0.607 ± 0.014	0.703 ± 0.009
$\omega_2 = 0$	0.849 ± 0.037	0.882 ± 0.029	0.736 ± 0.068	0.753 ± 0.064	0.718 ± 0.075	0.794 ± 0.050	0.849 ± 0.037
Proposed	0.988 ± 0.001	0.988 ± 0.001	0.975 ± 0.003	0.976 ± 0.003	0.974 ± 0.003	0.979 ± 0.002	0.988 ± 0.001
ORL	ACC	NMI	ARI	F1-score	Precision	Recall	Purity
$\alpha = 0$	0.979 ± 0.016	0.996 ± 0.003	0.979 ± 0.016	0.979 ± 0.016	0.966 ± 0.026	0.993 ± 0.006	0.984 ± 0.012
$\omega_1 = 0$	0.918 ± 0.000	0.977 ± 0.001	0.897 ± 0.009	0.900 ± 0.009	0.852 ± 0.016	0.954 ± 0.000	0.940 ± 0.000
$\omega_2 = 0$	0.980 ± 0.017	0.996 ± 0.003	0.980 ± 0.017	0.980 ± 0.017	0.968 ± 0.027	0.993 ± 0.006	0.985 ± 0.013
Proposed	1.000 ± 0.000						
UCI-digital	ACC	NMI	ARI	F1-score	Precision	Recall	Purity
$\alpha = 0$	0.996 ± 0.000	0.988 ± 0.000	0.990 ± 0.000	0.991 ± 0.000	0.991 ± 0.000	0.991 ± 0.000	0.996 ± 0.000
$\omega_1 = 0$	0.987 ± 0.000	0.973 ± 0.000	0.970 ± 0.000	0.973 ± 0.000	0.973 ± 0.000	0.974 ± 0.000	0.987 ± 0.000
$\omega_2 = 0$	0.996 ± 0.000	0.988 ± 0.000	0.990 ± 0.000	0.991 ± 0.000	0.991 ± 0.000	0.991 ± 0.000	0.996 ± 0.000
Proposed	0.998 ± 0.000	0.993 ± 0.000	0.994 ± 0.000	0.995 ± 0.000	0.995 ± 0.000	0.995 ± 0.000	0.998 ± 0.000
YaleB	ACC	NMI	ARI	F1-score	Precision	Recall	Purity
$\alpha = 0$	0.605 ± 0.003	0.619 ± 0.004	0.399 ± 0.006	0.463 ± 0.005	0.427 ± 0.005	0.505 ± 0.004	0.607 ± 0.003
$\omega_1 = 0$	0.138 ± 0.003	0.090 ± 0.003	0.001 ± 0.000	0.178 ± 0.000	0.099 ± 0.000	0.869 ± 0.003	0.153 ± 0.003
$\omega_2 = 0$	0.609 ± 0.003	0.624 ± 0.004	0.405 ± 0.005	0.468 ± 0.005	0.433 ± 0.005	0.510 ± 0.004	0.610 ± 0.003
Proposed	0.954 ± 0.002	0.908 ± 0.001	0.900 ± 0.003	0.910 ± 0.002	0.909 ± 0.003	0.912 ± 0.003	0.954 ± 0.003

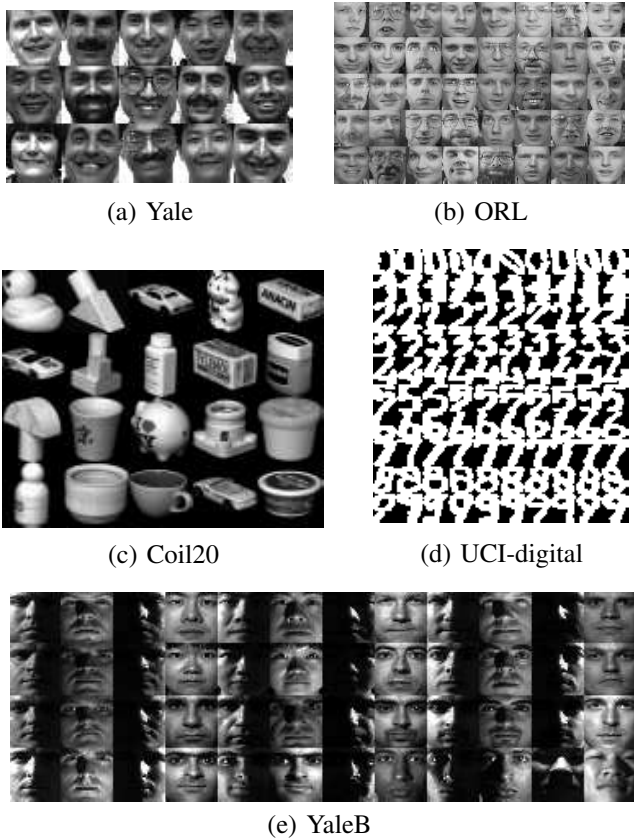


Fig. 2. Sample images from five datasets used in the experiments. (a) Yale, (b) ORL, (c) Coil20, (d) UCI-digital, and (e) YaleB.

perfect clustering results on Yale and UCI-digit. Specifically, on Yale, the ACC value of our model is 0.988, which means there are only two samples being wrongly partitioned by the proposed method on average. On UCI-digit, the ACC value is 0.998, indicating that only 4 samples are assigned to the incorrect groups among 2000 samples. On ORL and Coil20, all the samples can be clustered correctly. Clustering on YaleB is a quite challenging task due to the large variation of luminance. Fortunately, our method also achieves the best and surprising performance, i.e., all the clustering metrics exceed 0.90. On the contrary, all the metrics for the other methods are lower than 0.71. This means a dramatic improvement of the proposed model over the compared methods, e.g., our method improves the ARI value more than 65% when compared with the second best method. Moreover, the improvements of the proposed method on the other datasets are also significant. Different methods have different assumptions for input data, and may favor different datasets. For example, t-SVD-MSC achieves high values of various metrics on Yale and ORL, but relatively low values of those on Coil20. ETLMC performs good on UCI-digit, but bad on YaleB. Remarkably, our method consistently produces the best performance on all the datasets, validating the robustness of our methods to different datasets. In addition, our method also significantly outperforms SNN and TRPCA. The reason is that they are designed for general purposes without considering the special characteristics of MVSC, while the proposed TLRN is tailored to MVSC, leading to the superior clustering performance.

C. Visual Comparison of the Learned Similarity Matrix

Fig. 3 visualizes the similarity matrices learned by two tensor based MVSC methods (i.e., LT-MSC and t-SVD-MSC),

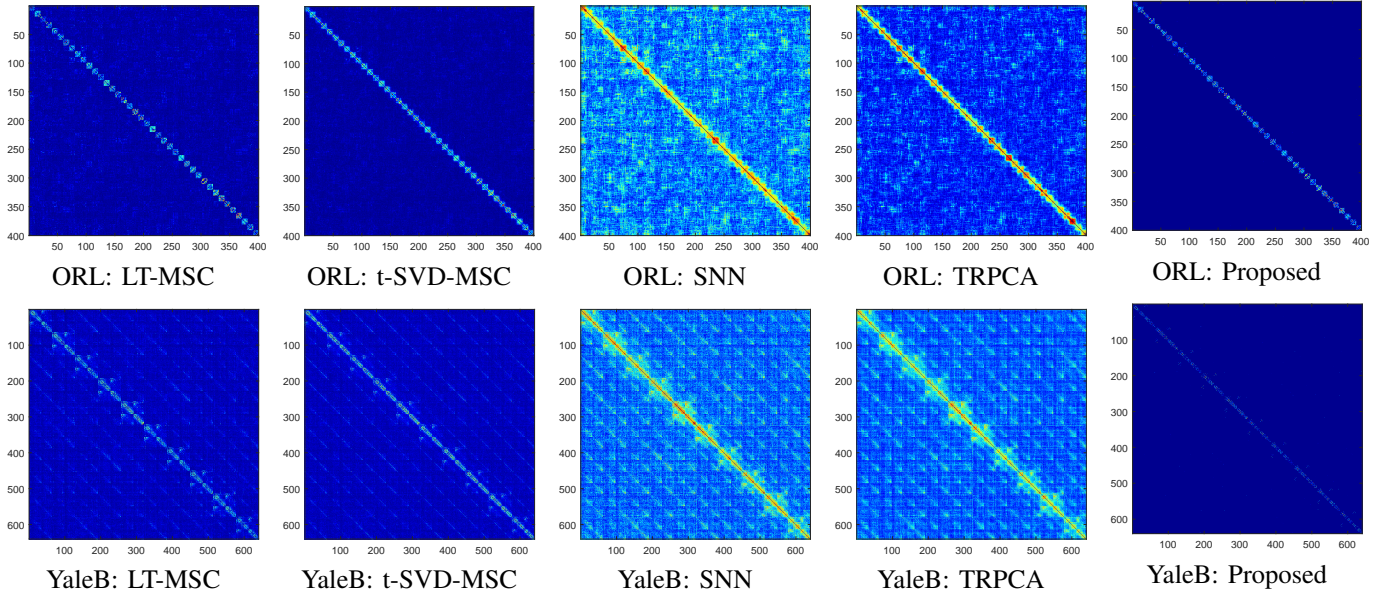


Fig. 3. Visual comparisons of the similarity matrices learned by different methods. It is clear that the connections of our method are distributed along the diagonal, and our method generates much fewer wrong connections than the compared methods.

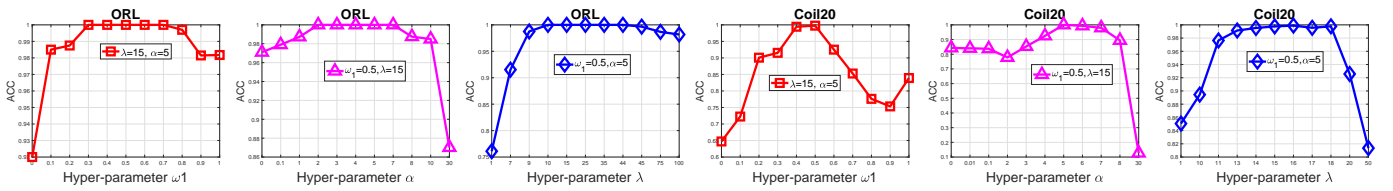


Fig. 4. Illustration of the effect of three hyper-parameters of our model (i.e., ω_1 , λ and α) on the clustering performance. It can be observed that the proposed method always achieves the highest performance in wide ranges of ω_1 , λ and α , demonstrating its robustness.

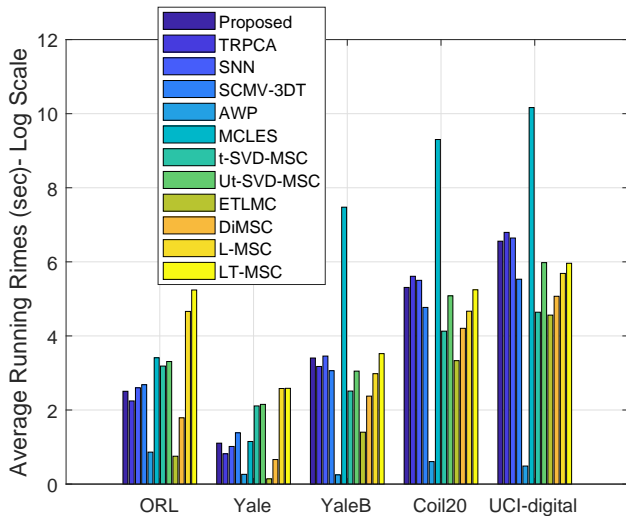


Fig. 5. Running time comparison of different methods on five datasets.

two TLRNs (i.e., SNN and TRPCA), and the proposed method. Compared with LT-MSC and t-SVD-MSC, the similarity matrix of our model shows a clear block-diagonal structure on ORL. On YaleB, there are many incorrect connections among

samples from different clusters in the similarity matrices by LT-MSC and t-SVD-MSC. On the contrary, the connections of the similarity matrix of the proposed method are sparsely distributed along the diagonal, indicating the majority of the connections are correct. The reason is that the proposed TLRN explicitly imposes a column-wise sparse regularization on the horizontal slices, such that it could remove the incorrect connections, while preserving the correct connections by exploring the cross view information. Such observations also explain why the proposed method can achieve the excellent clustering performance over others in Tables II-VI. In addition, compared with the two existing TLRNs, the recovered similarity matrices of SNN and TRPCA on both ORL and YaleB are quite dense. Conversely, the similarity matrices of our method are sparse, which is very important for SC [1]. The reason is that, unlike the existing TLRNs, the proposed TLRN takes the unique characteristics of MVSC into account.

D. Parameter Analysis

Fig. 4 shows how the three hyper-parameters involved in our model affect clustering performance. On ORL, we can observe that the highest ACC is achieved in a wide range of ω_1 around 0.5, i.e., $0.3 \leq \omega_1 \leq 0.7$, indicating that the modelings of both the horizontal slices and the frontal slices make contributions to the proposed model. The highest ACC of ORL occurs when

TABLE VIII
CLUSTERING PERFORMANCE OF OUR MODEL WITH DIFFERENT INITIAL AFFINITY MATRICES

ORL	ACC	NMI	ARI	F1-score	Precision	Recall	Purity
LT-MSC [13]	0.808 ± 0.022	0.915 ± 0.010	0.747 ± 0.029	0.753 ± 0.028	0.708 ± 0.034	0.805 ± 0.023	0.838 ± 0.015
Proposed (LT-MSC)	0.831 ± 0.018	0.950 ± 0.005	0.838 ± 0.015	0.841 ± 0.014	0.801 ± 0.020	0.886 ± 0.010	0.901 ± 0.013
ETLMC [17]	0.946 ± 0.018	0.986 ± 0.005	0.942 ± 0.020	0.943 ± 0.019	0.918 ± 0.026	0.970 ± 0.014	0.960 ± 0.014
Proposed (ETLMC)	0.960 ± 0.008	0.987 ± 0.003	0.952 ± 0.009	0.953 ± 0.009	0.936 ± 0.011	0.972 ± 0.008	0.969 ± 0.005
YaleB	ACC	NMI	ARI	F1-score	Precision	Recall	Purity
LT-MSC [13]	0.617 ± 0.002	0.623 ± 0.006	0.413 ± 0.006	0.491 ± 0.005	0.466 ± 0.005	0.521 ± 0.005	0.620 ± 0.002
Proposed (LT-MSC)	0.831 ± 0.002	0.778 ± 0.001	0.593 ± 0.003	0.638 ± 0.002	0.571 ± 0.003	0.723 ± 0.002	0.831 ± 0.002
ETLMC [17]	0.325 ± 0.011	0.307 ± 0.021	0.179 ± 0.019	0.262 ± 0.017	0.257 ± 0.017	0.267 ± 0.017	0.332 ± 0.010
Proposed (ETLMC)	0.452 ± 0.000	0.455 ± 0.000	0.177 ± 0.000	0.278 ± 0.000	0.224 ± 0.000	0.366 ± 0.000	0.455 ± 0.000
Yale	ACC	NMI	ARI	F1-score	Precision	Recall	Purity
LT-MSC [13]	0.739 ± 0.014	0.767 ± 0.009	0.597 ± 0.013	0.623 ± 0.012	0.601 ± 0.012	0.647 ± 0.014	0.739 ± 0.014
Proposed (LT-MSC)	0.780 ± 0.015	0.784 ± 0.016	0.540 ± 0.037	0.572 ± 0.033	0.507 ± 0.049	0.659 ± 0.010	0.780 ± 0.015
ETLMC [17]	0.677 ± 0.074	0.725 ± 0.062	0.558 ± 0.089	0.585 ± 0.083	0.572 ± 0.085	0.599 ± 0.082	0.677 ± 0.074
Proposed (ETLMC)	0.733 ± 0.071	0.769 ± 0.058	0.617 ± 0.088	0.641 ± 0.082	0.628 ± 0.086	0.656 ± 0.077	0.733 ± 0.072
UCI	ACC	NMI	ARI	F1-score	Precision	Recall	Purity
LT-MSC [13]	0.792 ± 0.009	0.762 ± 0.009	0.707 ± 0.014	0.737 ± 0.013	0.724 ± 0.012	0.749 ± 0.013	0.809 ± 0.009
Proposed (LT-MSC)	0.815 ± 0.003	0.765 ± 0.006	0.692 ± 0.007	0.723 ± 0.007	0.713 ± 0.008	0.732 ± 0.005	0.815 ± 0.003
ETLMC [17]	0.941 ± 0.023	0.970 ± 0.013	0.933 ± 0.029	0.936 ± 0.027	0.935 ± 0.032	0.938 ± 0.024	0.942 ± 0.019
Proposed (ETLMC)	0.997 ± 0.000	0.991 ± 0.000	0.992 ± 0.000	0.993 ± 0.000	0.993 ± 0.000	0.993 ± 0.000	0.997 ± 0.000
Coil20	ACC	NMI	ARI	F1-score	Precision	Recall	Purity
LT-MSC [13]	0.770 ± 0.013	0.873 ± 0.005	0.725 ± 0.018	0.740 ± 0.017	0.696 ± 0.027	0.790 ± 0.005	0.817 ± 0.005
Proposed (LT-MSC)	0.844 ± 0.013	0.941 ± 0.003	0.828 ± 0.010	0.837 ± 0.010	0.774 ± 0.014	0.912 ± 0.008	0.880 ± 0.006
ETLMC [17]	0.956 ± 0.037	0.977 ± 0.012	0.950 ± 0.035	0.952 ± 0.033	0.937 ± 0.049	0.969 ± 0.019	0.965 ± 0.027
Proposed (ETLMC)	0.988 ± 0.008	0.988 ± 0.004	0.977 ± 0.014	0.978 ± 0.013	0.975 ± 0.017	0.981 ± 0.009	0.988 ± 0.008

$\alpha \in [2, 7]$, suggesting that the $\ell_{2,1}$ norm is more important than the low-rank term in the horizontal slices. The proposed model is also robust to λ on ORL, i.e., the highest ACC occurs in a wide range of λ : $10 \leq \lambda \leq 44$. Moreover, on Coil20, the proposed model is also able to produce the highest ACC with a wide range of hyper-parameters. For the results shown in Tables II-VI, the selected hyper-parameters of the proposed model on all datasets are close to each other, and they all fall in the range where the highest ACC of ORL occurs, i.e., $\omega_1 \in [0.3, 0.7]$, $\alpha \in [2, 7]$, $\lambda \in [10, 44]$. All these observations validate that the hyper-parameters of our method are relatively easy to choose, which proves the practicability of our model.

E. Ablation Study

We also conducted ablation studies to comprehensively understand and evaluate the proposed model. First, we studied the effectiveness of the regularization terms contained in our model. As shown in Table VII, $\alpha = 0$, $\omega_1 = 0$ and $\omega_2 = 0$ denote the proposed model without considering the column-wise sparsity, the frontal low-rankness, and the horizontal structure, respectively. From Table VII, we can see that the clustering performance drops a lot when removing any regularization term contained in the proposed model, validating the effectiveness of each term. Specifically, $\omega_1 = 0$ usually produces the worst clustering performance. The reason is that the frontal slice of the tensor corresponds to the intra-view similarity relationship and further takes responsible for the final clustering task.

Second, as an initial similarity matrix is required in our method, we investigated the adaptation of the proposed model to different similarity matrix construction methods. Specifically, we used the outputs of LT-MSC [13] and ETLMC [17] as the initial similarity matrices of our method, and the corresponding methods are denoted as Proposed (LT-MSC) and

Proposed (ETLMC), respectively. As shown in Table VIII, it is obvious that Proposed (LT-MSC) (resp. Proposed (ETLMC)) can significantly improve the performance of LT-MSC (resp. ETLMC), which validates the robustness of our model to different initial similarity matrix construction methods. In other words, the proposed model can act as a post-processing technique to improve the performance of other existing MVSC methods.

F. Comparison of Running Time

Fig. 5 illustrates the running time of all the methods on five datasets, where all of them were implemented with MATLAB on a Windows computer with a 3.7GHz Intel(R) i7-8700k CPU and 32.0 GB memory. We reported the average running time of 20 trails. From Fig. 5, we can observe that the running time of our method is roughly at the same level as most methods under comparison, like SNN, TRPCA, and LT-MSC. Moreover, our method is much faster than MCLES on large datasets, including YaleB, Coil20 and UCI-digital. We can conclude that, compared with the state-of-the-art methods, our model is able to largely improve the clustering performance without increasing the running time.

V. CONCLUSION AND FUTURE WORK

In this paper, we have presented a novel tensor low-rank norm tailored to MVSC, which explicitly characterizes both the intra-view and inter-view of the multi-view samples. Based on that, we formulated the MVSC as a low-rank tensor learning problem, and solved it with an augmented Lagrange multiplier method. Our method is fundamentally different from the existing methods which simply employ an existing TLRN that is designed for general purposes. The experimental results on five commonly-used benchmark datasets have substantiated

the significant superiority of our model over eleven state-of-the-art MVSC methods, and validated the rationality of our modeling on the special characteristics of MVSC in low-rank tensor representation. Moreover, hyper-parameters of our model are relatively easy to determine, and our model is robust to different datasets and can adapt to different initial similarity matrices, validating its potential in practice. We believe our perspective on MVSC will inspire this community.

In the future, we will incorporate the proposed TLRN to a graph learning framework to learn a reasonable similarity matrix directly. Second, the proposed LRTN has the potential to solve the ensemble clustering problem, where different data partitions of ensemble clustering can act as multiple views. In addition, the final similarity matrix of our method used for clustering is achieved by simply averaging the output tensor along the frontal direction, and thus it is expected that more elegant and effective fusion methods would further boost the performance.

REFERENCES

- [1] U. von Luxburg, "A tutorial on spectral clustering," *Statistics and Computing*, vol. 17, no. 4, pp. 395–416, Dec 2007. [Online]. Available: <https://doi.org/10.1007/s11222-007-9033-z>
- [2] Z. Yue, H. Yong, D. Meng, Q. Zhao, Y. Leung, and L. Zhang, "Robust multiview subspace learning with nonindependently and nonidentically distributed complex noise," *IEEE Trans. Neural Netw. Learn. Syst.*, pp. 1–14, 2019.
- [3] K. Zhan, F. Nie, J. Wang, and Y. Yang, "Multiview consensus graph clustering," *IEEE Trans. Image Process.*, vol. 28, no. 3, pp. 1261–1270, March 2019.
- [4] R. Xia, Y. Pan, L. Du, and J. Yin, "Robust multi-view spectral clustering via low-rank and sparse decomposition," in *Proc. AAAI*, 2014.
- [5] X. Cao, C. Zhang, H. Fu, S. Liu, and H. Zhang, "Diversity-induced multi-view subspace clustering," in *Proc. IEEE CVPR*, 2015, pp. 586–594.
- [6] H. Zhao, Z. Ding, and Y. Fu, "Multi-view clustering via deep matrix factorization," in *Proc. AAAI*, 2017.
- [7] C. Zhang, Q. Hu, H. Fu, P. Zhu, and X. Cao, "Latent multi-view subspace clustering," in *Proc. IEEE CVPR*, 2017, pp. 4279–4287.
- [8] X. Wang, X. Guo, Z. Lei, C. Zhang, and S. Z. Li, "Exclusivity-consistency regularized multi-view subspace clustering," in *Proc. IEEE CVPR*, 2017, pp. 923–931.
- [9] Y. Yang and H. Wang, "Multi-view clustering: A survey," *Big Data Mining and Analytics*, vol. 1, no. 2, pp. 83–107, June 2018.
- [10] Y. Li, M. Yang, and Z. Zhang, "A survey of multi-view representation learning," *IEEE Trans. Knowl. Data Eng.*, vol. 31, no. 10, pp. 1863–1883, Oct 2019.
- [11] J. Zhao, X. Xie, X. Xu, and S. Sun, "Multi-view learning overview: Recent progress and new challenges," *Information Fusion*, vol. 38, pp. 43–54, 2017.
- [12] M. Yin, J. Gao, S. Xie, and Y. Guo, "Multiview subspace clustering via tensorial t-product representation," *IEEE Trans. Neural Netw. Learn. Syst.*, vol. 30, no. 3, pp. 851–864, March 2019.
- [13] C. Zhang, H. Fu, S. Liu, G. Liu, and X. Cao, "Low-rank tensor constrained multiview subspace clustering," in *Proc. ICCV*, 2015, pp. 1582–1590.
- [14] J. Liu, P. Musialski, P. Wonka, and J. Ye, "Tensor completion for estimating missing values in visual data," *IEEE Trans. Pattern Anal. Mach. Intell.*, vol. 35, no. 1, pp. 208–220, Jan 2013.
- [15] Y. Xie, D. Tao, W. Zhang, Y. Liu, L. Zhang, and Y. Qu, "On unifying multi-view self-representations for clustering by tensor multi-rank minimization," *Int. J. Comput. Vis.*, vol. 126, no. 11, pp. 1157–1179, 2018.
- [16] M. E. Kilmer, K. Braman, N. Hao, and R. C. Hoover, "Third-order tensors as operators on matrices: A theoretical and computational framework with applications in imaging," *SIAM J. Matrix Anal. Appl.*, vol. 34, no. 1, pp. 148–172, 2013.
- [17] J. Wu, Z. Lin, and H. Zha, "Essential tensor learning for multi-view spectral clustering," *IEEE Trans. Image Process.*, vol. 28, no. 12, pp. 5910–5922, 2019.
- [18] Y. Qu, J. Liu, Y. Xie, and W. Zhang, "Robust kernelized multi-view self-representations for clustering by tensor multi-rank minimization," *arXiv preprint arXiv:1709.05083*, 2017.
- [19] Y. Tang, Y. Xie, X. Yang, J. Niu, and W. Zhang, "Tensor multi-elastic kernel self-paced learning for time series clustering," *IEEE Trans. Knowl. Data Eng.*, pp. 1–1, 2019.
- [20] Y. Liu, Z. Long, H. Huang, and C. Zhu, "Low cp rank and tucker rank tensor completion for estimating missing components in image data," *IEEE Trans. Circuits Syst. Video Technol.*, vol. 30, no. 4, pp. 944–954, 2020.
- [21] Y. Liu, J. Liu, and C. Zhu, "Low-rank tensor train coefficient array estimation for tensor-on-tensor regression," *IEEE Trans. Neural Netw. Learn. Syst.*, pp. 1–10, 2020.
- [22] Y. Liu, Z. Long, H. Huang, and C. Zhu, "Low cp rank and tucker rank tensor completion for estimating missing components in image data," *IEEE Trans. Circuits Syst. Video Technol.*, vol. 30, no. 4, pp. 944–954, 2020.
- [23] C. J. Hillar and L.-H. Lim, "Most tensor problems are np-hard," *Journal of the ACM (JACM)*, vol. 60, no. 6, pp. 1–39, 2013.
- [24] C. Lu, J. Feng, Y. Chen, W. Liu, Z. Lin, and S. Yan, "Tensor robust principal component analysis with a new tensor nuclear norm," *IEEE Trans. Pattern Anal. Mach. Intell.*, vol. 42, no. 4, pp. 925–938, 2020.
- [25] Z. Zhang, G. Ely, S. Aeron, N. Hao, and M. Kilmer, "Novel methods for multilinear data completion and de-noising based on tensor-svd," in *Proc. IEEE CVPRn*, 2014, pp. 3842–3849.
- [26] F. Nie, L. Tian, and X. Li, "Multiview clustering via adaptively eighted procrustes," in *Proc. ACM SIGKDD*, 2018, pp. 2022–2030.
- [27] A. Kumar, P. Rai, and H. Daume, "Co-regularized multi-view spectral clustering," in *Proc. NIPS*, 2011, pp. 1413–1421.
- [28] A. Kumar and H. Daumé, "A co-training approach for multi-view spectral clustering," in *Proc. ICML*, 2011, pp. 393–400.
- [29] Z. Yang, Q. Xu, W. Zhang, X. Cao, and Q. Huang, "Split multiplicative multi-view subspace clustering," *IEEE Trans. Image Process.*, vol. 28, no. 10, pp. 5147–5160, 2019.
- [30] C. Zhang, H. Fu, Q. Hu, X. Cao, Y. Xie, D. Tao, and D. Xu, "Generalized latent multi-view subspace clustering," *IEEE Trans. Pattern Anal. Mach. Intell.*, vol. 42, no. 1, pp. 86–99, Jan 2020.
- [31] M.-S. Chen, L. Huang, C.-D. Wang, and D. Huang, "Multi-view clustering in latent embedding space," in *Proc. AAAI*, 2020.
- [32] C. Zhang, H. Fu, J. Wang, W. Li, X. Cao, and Q. Hu, "Tensorized multi-view subspace representation learning," *Int. J. Comput. Vis.*, pp. 1–18, 2020.
- [33] X. Xiao, Y. Chen, Y. Gong, and Y. Zhou, "Prior knowledge regularized multiview self-representation and its applications," *IEEE Trans. Neural Netw. Learn. Syst.*, pp. 1–14, 2020.
- [34] E. J. Candès, X. Li, Y. Ma, and J. Wright, "Robust principal component analysis?" *J. ACM*, vol. 58, no. 3, Jun. 2011. [Online]. Available: <https://doi.org/10.1145/1970392.1970395>
- [35] Z. Lin, M. Chen, and Y. Ma, "The augmented lagrange multiplier method for exact recovery of corrupted low-rank matrices," *arXiv preprint arXiv:1009.5055*, 2010.
- [36] Z. Lin, R. Liu, and Z. Su, "Linearized alternating direction method with adaptive penalty for low-rank representation," in *Proc. NIPS*, 2011, pp. 612–620.
- [37] M. Lyons, S. Akamatsu, M. Kamachi, and J. Gyoba, "Coding facial expressions with gabor wavelets," in *Proc. IEEE FG. IEEE*, 1998, pp. 200–205.
- [38] T. Ahonen, A. Hadid, and M. Pietikainen, "Face description with local binary patterns: Application to face recognition," *IEEE Trans. Pattern Anal. Mach. Intell.*, no. 12, pp. 2037–2041, 2006.
- [39] A. Y. Ng, M. I. Jordan, and Y. Weiss, "On spectral clustering: Analysis and an algorithm," in *Proc. NIPS*, 2002, pp. 849–856.